Entropy **2013**, *15*, 4716-4731; doi:10.3390/e15114716

OPEN ACCESS

entropy

ISSN 1099-4300

www.mdpi.com/journal/entropy

Article

Optimal Thermal Design of a Stacked Mini-Channel Heat Sink Cooled by a Low Flow Rate Coolant

Liping Pang *, Minxing Wang, Wei Wang, Meng Liu and Jun Wang

School of Aviation Science and Engineering, Beijing University of Aeronautics and Astronautics, Xueyuan Road 37, Haidian District, Beijing 100191, China; E-Mails: zwq8282@163.com (M.W.); vidvi.wong@gmail.com (W.W.); liumeng@buaa.edu.cn (M.L.); wangjun@buaa.edu.cn (J.W.)

* Author to whom correspondence should be addressed; E-Mail: pangliping@buaa.edu.cn; Tel./Fax: +86-10-8231-3186.

Received: 15 August 2013; in revised form: 15 October 2013 / Accepted: 24 October 2013 / Published: 31 October 2013

Abstract: Application requirements for avionics are often very strict. For example, the heat sinks of avionics need very good temperature uniformity, but the flow rate of coolant is very restricted. In addition, the use of micro-channels is not recommended due to the potential clogging issue. Considering these design requirements, we will discuss a multiple-objective optimal design method to obtain a good stacked mini-channel structure for avionics applications. In our thermal design, the design variables are the mini-channel geometry parameters. Temperature uniformity, entropy generation, max temperature of heat sink and pump work are chosen as the objective functions. A Multi Objective Genetic Algorithm (MOGA) and Fluent solver are used together to minimize multiple objective functions subject to constraints, and locate the Pareto front. By analyzing the multiple objective optimal results, we can draw the conclusion that the objective functions of T_{max} and s_g have same effect on the optimization, and the multiple optimal results are a set and not a single value. If mostly focusing on the temperature uniformity, we can recommend some optimal structures to design a stacked mini-channel heat sink.

Keywords: mini-channel heat sink; entropy generation minimization; optimization; Pareto-optimal solutions

---

1. Introduction

The effective removal of the generated heat is very important for electronic devices, especially for avionics, to ensure a safe operating temperature of these devices. Liquid cooled micro- and mini-channel heat sinks have received much attention because of their ability to dissipate heat fluxes [1–3]. Single layer micro-channel heat sinks have been the most extensively studied form, but stacked multi-layer micro- or mini-channel heat sinks may have significant advantages because they can offer a high thermal performance with tolerable pressure drop and low flow rates. Some studies on multi layer micro- and mini-channel heat sinks have been conducted [4–12]. They showed that the overall thermal resistance for a two layered micro-channel stack was 30 percent less than for the single layered micro-channel due to doubling of the heat transfer area, even though the dimensions of micro-channel were not optimized.

Some researchers have considered the optimization of micro- or mini-channels as a multi-objective optimization rather than a single-objective optimization. The pressure drop, the Nusselt number of the flow and performances of heat transfer in micro- and mini-channels are mostly chosen as objective functions. These objective functions are either obtained from experiments or computed using very timely and high-cost computer fluid dynamic (CFD) approaches [8,13–15].

Multi-objective optimization techniques in combination with genetic algorithms have also been proven to be suitable solution methods for problems where multiple criteria must be satisfied, as they result in concurrent optimization of all the objectives [16,17]. The vector evaluated genetic algorithm, Fonseca and Fleming's genetic algorithm (MOGA), the non-dominated sorting genetic algorithm (NSGA) were all used.

The objective of this paper was to search for an optimal thermal design structure for a stacked mini-channel heat sink in order to obtain a good temperature uniformity cooled by low flow rate coolant. A Multi Objective Genetic Algorithm (MOGA) and Fluent solver are used together to minimize multiple objective functions subject to constraints, and locate the Pareto front.

2. Thermal Design Object

2.1. Structure and Constrained Conditions

Our thermal design for heat sink of avionics has the following features: high temperature uniformity, small quantity of coolant and high operational reliability, so a mini-channel heat sink structure is adopted to cool the avionics.

Figure 1 shows a typical avionics heat source structure. It is a rectangular shape, with a uniform heat flux, $q_1 = 10^5$ W·m^{-2} over it. The width and length of the cold plane are limited by L_e and W_e; here L_e is length and W_e is width. In our thermal design, $L_e = 0.15$ m, $W_e = 0.1$ m.

Figure 1. Typical avionics heat source and its cold plate.

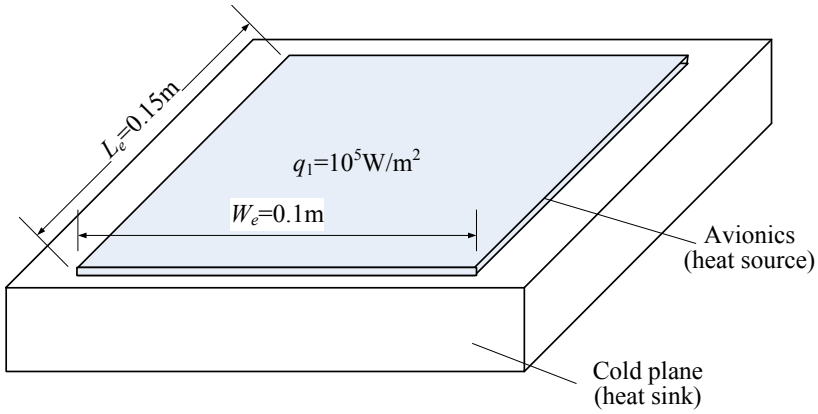

In this thermal design, some conditions are strictly constrained:

(1) Water coolant requirement:

Flow rate is 0.08318 kg·s^{-1}, inlet temperature is 313 K and outlet temperature is less than 333 K.

(2) Heat source surface temperature uniformity requirement:

Temperature difference between the max and min temperatures of the cooled heat source surface is less than 3 K.

(3) Mini-channel geometry requirement:

The width and height of mini-channel should satisfy $w \geq 0.5$ mm and 2 mm $\leq h \leq$ 10 mm, respectively. The number of mini-channels in every layer satisfies $20 \leq n \leq 80$. The geometry of mini-channel is relatively large comparing to micro-channel.

Considering the above design requirements, a stacked mini-channel heat sink structure was finally adopted, as shown in Figure 2. The width and height of the designed mini-channel cold plane are constrained to W_e and L_e. The coolant is arranged to counter flow into a two-layer mini-channel structure in order to satisfy the temperature uniformity requirement. The geometry parameters for the first and second layers are $h_1 \times w_1$, and $h_2 \times w_2$, respectively.

Figure 2. Geometry parameters of a stacked mini-channel heat sink with a counter flow arrangement.

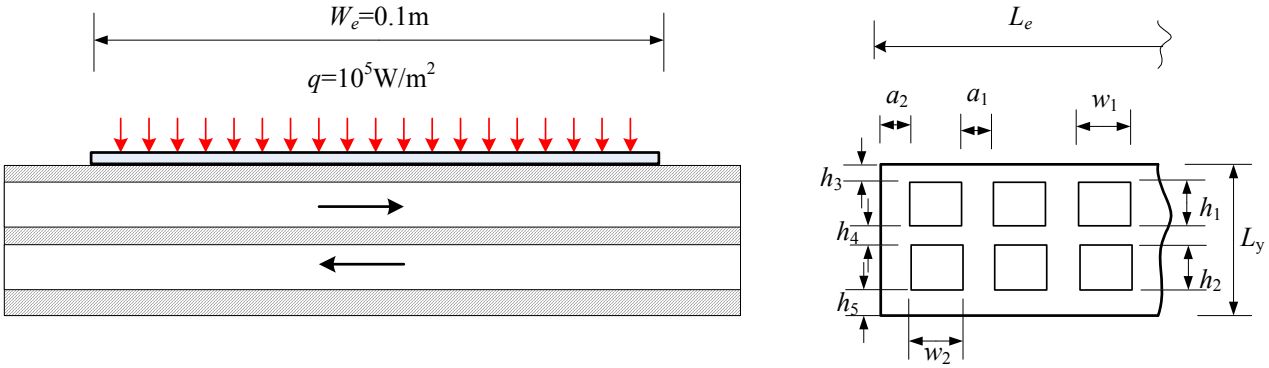

2.2. Flow and Heat Transfer Model

Because the geometry of mini-channels is on the order of millimeters, a computational fluid dynamics (CFD) code can be used to solve the governing equations and numerically simulate the flow through mini-channels [13,18]. In numerical analysis, a single mini-channel domain with full flow length is used due to the computational load and time consumption, as shown in Figure 3. We let h_3 = 1 mm, h_4 = 1 mm, h_5 = 1 mm, and a_2 = 0.5 mm. The value of a_1 is decided by n. In addition, we let $w_2 = w_1$ and $h_2 = h_1$, so h_1, w_1, and n are the final optimized variables in our thermal design. When a set of (h_1, w_1, n) is given, we can use Fluent solver to obtain the numerical computation results.

Figure 3. Computation domain of mini-channel.

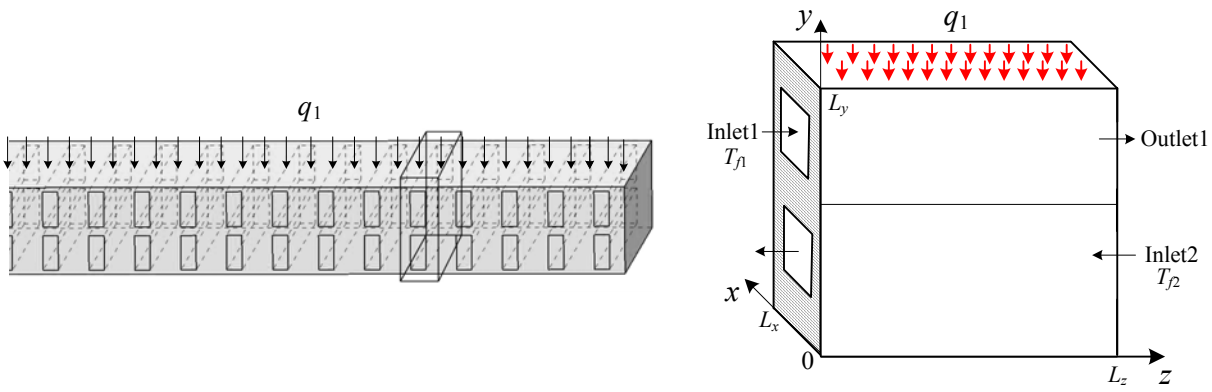

In this thermal design, the coolant flow is assumed to be laminar, steady and incompressible. The radiation of cold plate is neglected. The fluid thermo-physical properties vary with temperature. Based on the above assumptions, the following governing equations for mass, momentum and energy balances are applied in the mini-channel fluid and solid regions:

Continuity:
$$\nabla\left(\rho_f \vec{\mathbf{u}}\right) = 0 \tag{1}$$

Momentum:
$$\vec{\mathbf{u}} \cdot \nabla(\rho_f \vec{\mathbf{u}}) = -\nabla p + \nabla \cdot (\mu_f \nabla \vec{\mathbf{u}}) \tag{2}$$

Energy:
$$\vec{\mathbf{u}} \cdot \nabla(\rho_f C_{p,f} T_f) = \nabla(k_f \nabla T_f) \text{ (for the fluid)} \tag{3}$$
$$\nabla \cdot (k_s \nabla T_s) = 0 \text{ (for the solid)} \tag{4}$$

where $\vec{\mathbf{u}}$ is fluid velocity vector, $\mathrm{m \cdot s^{-1}}$; p is fluid pressure, Pa; T_f and T_s are fluid and solid temperature, respectively; μ_f, ρ_f, k_f, $C_{p,f}$ are the viscosity, density, thermal conductivity, specific heat of the fluid, respectively; k_s is the thermal conductivity of the solid.

2.3. Boundary Conditions

A uniform heat flux, q_1, is applied at $y = L_y$ in Figure 3. The boundary at $y = 0$ was assumed to be adiabatic. Due to the symmetry conditions at planes $x = 0$ and $x = L_x$, these planes are taken to be adiabatic conditions.

In the fluid region, the coolant is assumed to enter the two-layer mini-channels at uniform temperatures, T_{f1} and T_{f2}, respectively. A uniform liquid mass flow rate is assumed at the channels' inlet. A constant fluid pressure, 300 Pa, and a zero temperature gradient are assumed at channels' exit. Continuity conditions of the temperature and the heat flux, as well as zero velocities are satisfied at all solid-fluid interfaces. A no-slip condition was applied at the interior walls of the micro-channels. So the boundary conditions are:

(1) Solid wall:

$$-k_s \frac{\partial T_s}{\partial y}\Big|_{y=Ly} = q_1$$

$$-k_s \frac{\partial T_s}{\partial y}\Big|_{y=0} = 0$$

$$-k_s \frac{\partial T_s}{\partial x}\Big|_{x=0 \text{ and } x=Lx} = 0$$

(2) Lower channel:

$$u_z = \dot{m}_2 / (\rho_f \cdot n \cdot h_1 \cdot w_1),\ u_x = u_y = 0,\ T_f = T_{f2},\ \text{at } z = L_z$$

$$\frac{\partial u}{\partial z} = u_x = u_y = 0,\ \frac{\partial T_f}{\partial z} = 0,\ \text{at } z = 0$$

$$u_z = u_x = u_y = 0,\ \text{at } x = \frac{a_1}{2},\ x = L_x - \frac{a_1}{2},\ y = h_5 \text{ and } y = h_5 + h_2$$

(3) Upper channel:

$$u_z = \dot{m}_1 / (\rho_f \cdot n \cdot h_2 \cdot w_2),\ u_x = u_y = 0,\ T_f = T_{f1},\ \text{at } z = 0$$

$$\frac{\partial u}{\partial z} = u_x = u_y = 0,\ \frac{\partial T_f}{\partial z} = 0,\ \text{at } z = L_z$$

$$u_z = u_x = u_y = 0,\ \text{at } x = \frac{a_1}{2},\ x = L_x - \frac{a_1}{2},\ y = h_5 + h_2 + h_4 \text{ and } y = L_y - h_3$$

(4) Solid and fluid interface:

$$u_x = u_y = u_z = 0,\ -k_f \frac{\partial T_f}{\partial y} = -k_s \frac{\partial T_s}{\partial y},\ -k_f \frac{\partial T_f}{\partial x} = -k_s \frac{\partial T_s}{\partial x}$$

3. Thermal Optimization Design of Stacked Mini-Channel Heat Sink

3.1. Objective Functions and Constraints

A system can be optimized through a multi-objective optimization with constraints. In our thermal optimal design, the objective functions are determined as follows:

(1) Temperature uniformity: $\min(\Delta T_s) = \min(T_{s,\max} - T_{s,\min})\Big|_{y=L_y}$

(2) Entropy production s_g: $\min(s_g)$

(3) Max temperature of heat source: $\min(T_{s,\max})\Big|_{y=L_y}$

(4) Pumping power w_{pump}: $\min(w_{pump})$

Considering the objective functions, we can obtain the vector:

$$\vec{f}(\vec{x}) = \left[f_1(\vec{x}), f_2(\vec{x}), f_3(\vec{x}), f_4(\vec{x}) \right] \tag{5}$$

where the competing objective functions $f_1(\vec{x})$, $f_2(\vec{x})$, $f_3(\vec{x})$ and $f_4(\vec{x})$ represent ΔT_s, s_g, $T_{s,max}$ and w_{pump}, respectively. $\vec{x}$ denotes the design variables, and represents the mini-channel geometry:

$$\vec{x} = \left[x_1, x_2, x_3, x_4, x_5 \right] \tag{6}$$

where x_1, x_2, x_3, x_4, x_5 represent w_1, h_1, w_2, h_2, n, respectively. The geometry parameters of upper mini-channels should satisfy $w_1 \geq 0.5$ mm and 2 mm $\leq h_1 \leq$ 10 mm. For the lower mini-channel, $w_2 = w_1$ and $h_2 = h_1$. The number of upper and lower mini-channels is same and equal to n, and n satisfies $20 \leq n \leq 80$.

The goal of optimization is to minimize the objective vector $\vec{f}(\vec{x})$ [19,20]. So the discussed multi-objective optimization question can be written as:

$$\begin{aligned} &\min_{\vec{x}} \vec{f}(\vec{x}) = \left[s_g(\vec{x}), T_{s,\max}(\vec{x}), \Delta T_s(\vec{x}), w_{pump}(\vec{x}) \right] \\ &\text{subject to} \quad \vec{g}(\vec{x}) \leq 0 \quad \textit{and} \quad \vec{h}(\vec{x}) = 0 \end{aligned} \tag{7}$$

where $\vec{g}(\vec{x})$ and $\vec{h}(\vec{x})$ are the vector functions that contain inequality and equality constraints functions, respectively.

In our study, the constraint functions are following:

- $g_1(\vec{x})$ is coolant outlet temperature: $T_{f,out} \leq 333$ K;
- $h_1(\vec{x})$ is coolant mass flux: $m_c = 0.08318$ kg·s^{-1};
- $h_2(\vec{x})$ is coolant inlet temperature: $T_{f1} = T_{f2} = 313$ K.

3.1.1. Entropy Generation of Stacked Mini-Channel Heat Sink

In this optimal thermal design, the entropy generation minimization is used as an objective function, so an entropy generation formula will be deduced for the stacked mini-channel heat sink. The irreversibility of this system includes heat transfer across the finite temperature difference and friction in two stacked mini-channels. The rate of entropy generation within a mini-channel structure is given as [21–23]:

$$s_g = s_{g,h} + s_{g,f} \tag{8}$$

where s_g is the rate of entropy generation, J·(kg·K)$^{-1}$; $s_{g,h}$ and $s_{g,f}$ are the entropy generation rates due to heat transfer and fluid friction. A control volume, as shown in Figure 4, is selected for developing the entropy generation model for the stacked mini-channel heat sink.

The average wall temperatures of the upper and lower channels are assumed to be T_{b1} and T_{b1}, respectively. T_{f1} and T_{f2} are inlet and outlet coolant temperature, respectively. The heat flux over the top of upper channel is q_1. The average heat flux from the upper channel to the lower channel is assumed to be q_2. The bottom of lower channel is regarded as impermeable and adiabatic.

Figure 4. Parameters of inlet and outlet of the stacked mini-channels.

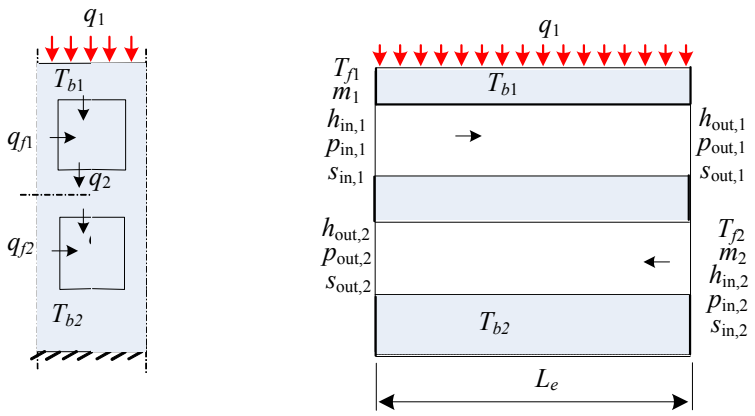

Let $\dot{m}_1 = \dot{m}_2$, and the mass rate balance for the steady state is:

$$\dot{m}_1 + \dot{m}_2 = \dot{m}_c \tag{9}$$

where subscript "1" and "2" represent upper and lower mini-channel, respectively; $\dot{m}$ is coolant flow rate in the mini-channels, kg·s^{-1}.

Energy satisfies:

$$q_1 = q_{b1} + q_{f1} + q_2 \,;\; q_2 = q_{b2} + q_{f2} \tag{10}$$

where q_f is the heat flow from the fin to fluid, W·m^{-2}; q_b is the heat flow from the base to fluid, W·m^{-2}.

For steady state, the entropy generation rate balance reduces to:

$$s_{g,1} = \dot{m}_1 (s_{out,1} - s_{in,1}) - \frac{q_{b1}}{T_{b1}} - \frac{q_{f1}}{T_{b1}} + \frac{q_2}{T_{b2}} \tag{11}$$

$$s_{g,2} = \dot{m}_2 (s_{out,2} - s_{in,2}) - \frac{q_2}{T_{b2}} \tag{12}$$

where subscript "in" and "out" represent inlet and outlet, respectively; T_b is the average temperature of heat source in the mini-channel, K.

Let $s_{in,1} = s_{in,2}$, and the total entropy generation can be reduced from Equations (10)–(12):

$$s_g = s_{g,1} + s_{g,2} = \dot{m}_1 (s_{out,1} - s_{in,1}) + \dot{m}_2 (s_{out,2} - s_{in,1}) - \frac{q_1 - q_2}{T_{b1}} \tag{13}$$

Integrating Gibb's equation from the inlet to the outlet and using the first law of thermodynamics for a steady-state condition [23], we can obtain Equations (14) and (15) for the upper mini-channel:

$$s_{out,1} - s_{in,1} = \frac{h_{out,1} - h_{in,1} - \Delta p_1 / \rho_f}{T_{f1}} \tag{14}$$

$$h_{out,1} - h_{in,1} = \frac{q_1 - q_2}{\dot{m}_1} \tag{15}$$

So:

$$s_{out,1} - s_{in,1} = \frac{q_1 - q_2}{m_1 \cdot T_{f1}} - \frac{\Delta p_1}{\rho_f \cdot T_{f1}} \tag{16}$$

where h is enthalpy, J·kg^{-1}; Δp is the pressure difference from inlet and outlet, Pa.

Similarly, for the lower mini-channel:

$$s_{out,2} - s_{in,1} = \frac{q_2}{m_2 \cdot T_{f2}} - \frac{\Delta p_2}{\rho \cdot T_{f2}} \tag{17}$$

From Equations (13), (14) and (15), and assume $T_{f1} = T_{f2} = T_f$ and $\Delta p_1 \approx \Delta p_2 = \Delta p$, we can reduce:

$$s_g = \left[q_1 \left(\frac{1}{T_f} - \frac{1}{T_{b1}} \right) + \frac{q_2}{T_{b1}} \right] + \frac{\Delta p \cdot \dot{m}_c}{\rho_f \cdot T_f} \tag{18}$$

3.1.2. Pumping Power

The power consumption is evaluated simply by Equation (17):

$$w_{pump} = G \cdot \Delta p \tag{1}$$

where G is volumetric flow rate, $m^3 \cdot s^{-1}$; Δp is the total pressure drop, pa; w_{pump} is pump power, W.

3.2. Optimal Procedure

Unlike single objective optimization, the solution of multi-objective optimization is not a single value, but rather a set of points known as the Pareto-optimal set. Each element in the Pareto-optimal set constitutes a non-inferior solution to the multi-objective optimization, and they are distributed along the Pareto-optimal front [24,25].

Figure 5. Optimization procedure by using MOGA.

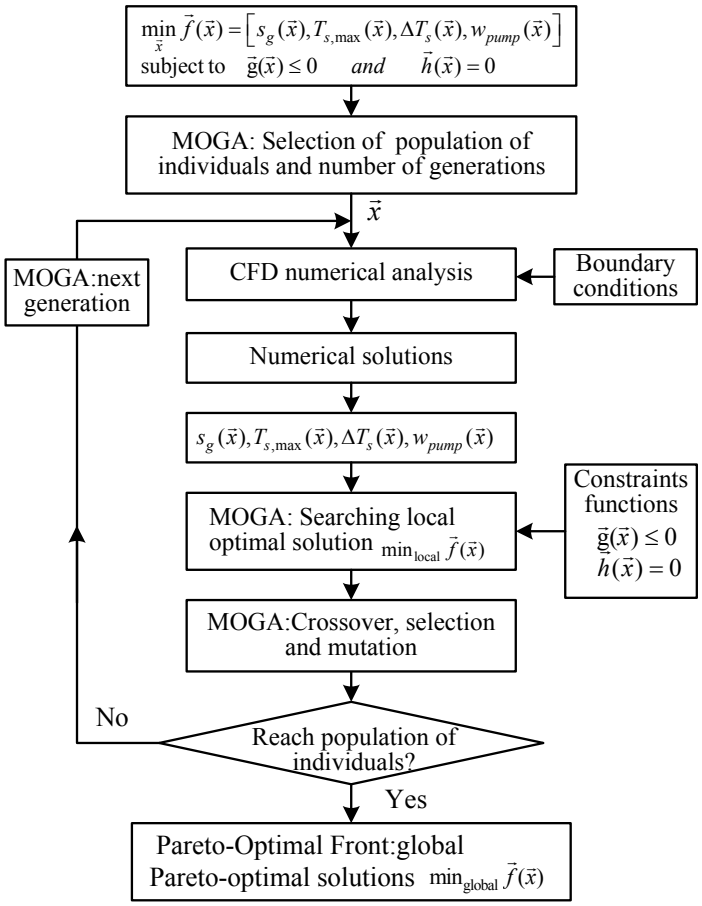

In order to locate the Pareto front, a Multi Objective Genetic Algorithm (MOGA) in modeFRONTIER V4.3 produced by ESTECO is used [26]. This algorithm repeatedly modifies a population of design variable vectors $\vec{x}_i$ according to the design requirement. At each optimal step, individuals of the current population are selected to produce off-springs for the next generation. The selection procedure is based on the objective function values and constraints functions. The MOGA to obtain the global Pareto-Optimal Front (POF) is shown in Figure 5.

In Figure 5, the crossover, selection and mutation are very important processes for the MOGA [19]. The directional crossover is a special operator which assumes that a direction of improvement can be detected comparing the fitness values of the individuals. The direction of evolutionary improvement is evaluated by comparing the fitness of the individual *i* with the fitness of two other individuals belonging to the same generation and selected with two different random walks. The new individual is then created moving in a randomly weighted direction that lies within the ones characterized by the given individual and the other two. The DNA string mutation ratio gives the percentage of the individual DNA that has to be changed by the mutation operator [26].

3.3. Numerical Solution and Calculation Grid

The continuity, momentum, and energy equations can be solved by a CFD software, Fluent [27]. Finite Volume Method (FVM) was used to convert the governing equations. The standard scheme for pressure discretization and SIMPLE algorithm for pressure velocity coupling were used. The type of difference for momentum and energy was second order upwind.

We used a simulation case to check the reliability of the numerical method. This simulation case is a smooth stacked rectangular channel with a single-phase flow. There is a constant heat flow, 8922.96 $W \cdot m^{-2}$, over the first channel. The width, height and length of channel are w = 0.9 mm, h = 1.8 mm and l = 100 mm, respectively. Since the ratio of the channel length to the hydraulic diameter, l/d_e, was greater than 70, the entrance effect of laminar flow can be ignored and the flow can be assumed as a fully developed laminar flow. By using the above numerical method, we obtained the average Nusselt number and $\overline{Nu}$ = 3.83, which was very near the one by Shah and London, 4.12 [28]. Due to the second layer channel can have a cooling effect for the first layer, this leads to the numerical value less than the theoretical one.

A completely orthogonal hexahedral mesh was utilized in our numerical calculation. We hope to obtain the max mesh sizes in the fluid and solid region, respectively, so that we can reduce our computation load. In order to obtain the grid independent solution, we tested some calculation cases by using some different grid densities in the fluid and solid regions. The solid material of mini-channel is copper.

The fluid regions in the tested four cases were 5 mm × 2 mm, 0.5 mm × 20 mm, 1 mm × 2 mm, 1 mm × 20 mm. In every case, the max grid step for solid region was set as 0.2 mm, 0.3 mm, 0.4 mm, 0.5 mm and 0.6 mm, respectively. The max grid step for fluid region was set as 0.03 mm, 0.05 mm, 0.1 mm and 0.2 mm respectively. Table 1 only shows the calculation results for n = 20 and the 5 mm × 2 mm fluid region.

Table 1. Grid independent study.

No.	Δl_s [$\times 10^{-3}$ m]	Δl_f [$\times 10^{-3}$ m]	N	$\Delta\tilde{T}_s$ [−]	$\tilde{T}_{s,\max}$ [−]	$\tilde{T}_{f,exit}$ [−]
1	0.3	0.2	133560	0.5191	1.0001	0.9938
2		0.1	179928	0.8161	0.9970	0.9978
3		0.05	271320	1.0000	1.0000	1.0000
4		0.03	451584	1.0070	1.0002	1.0007
5	0.6	0.05	78540	0.9794	1.0002	1.0001
6	0.5		104535	0.9784	0.9999	1.0000
7	0.4		149184	0.9788	0.9968	0.9989
8	0.3		271320	1.0000	1.0000	1.0000
9	0.2		620472	1.0015	0.9999	1.0000

In Table 1, N is the total number of grids for solid and fluid region. Δl_s and Δl_f are the max grid steps for solid and fluid regions, respectively. $\Delta\tilde{T}_s$, $\tilde{T}_{s,\max}$ and $\tilde{T}_{f,exit}$ are dimensionless numbers, and are defined as follows:

$$\Delta\tilde{T}_s = \Delta T_s\Big|_{\Delta l_s,\Delta l_f} / \Delta T_s\Big|_{\Delta l_{s=0.3},\Delta l_{f=0.05}}$$

$$\tilde{T}_{s,\max} = T_{s,\max}\Big|_{\Delta l_s,\Delta l_f} / T_{s,\max}\Big|_{\Delta l_{s=0.3},\Delta l_{f=0.05}}$$

$$\tilde{T}_{s,exit} = T_{s,exit}\Big|_{\Delta l_s,\Delta l_f} / T_{s,exit}\Big|_{\Delta l_{s=0.3},\Delta l_{f=0.05}}$$

From Table 1 we can know that when the number of the grids is over 271,320, the mesh independence solution can be obtained. At this time, the grid sizes for the fluid region and solid region are 0.05 mm and 0.3 mm, respectively.

We also analyze the other cases in the same way, and get the following conclusion: for the studied calculation conditions, $w_1 \geq 0.5$ mm and 2 mm $\leq h_1 \leq$ 10 mm and $20 \leq n \leq 80$, the grid independent solution can be obtained when the grid sizes for the fluid region and solid region are 0.05 mm and 0.3 mm, respectively.

In our study, coupling the genetic algorithm to a full 3D numerical model will result to a time consuming procedure. For our study as shown in Figure 3, when the parameters of MOGA listed in Table 1 are adopted, the total CPU time required for the whole optimal algorithm is 24.17 h. The computer configuration for optimization is as follows:

- CPU: Intel core 2Quad CPU, Q8400, 2.66 GHz;
- Memory is 3.2 G.

4. Optimization Results

4.1. Optimization Conditions

Based on the optimization method described in the above section, the Pareto-optimal solutions can be obtained for global optimization by using MOGA and Fluent solver together. The termination

condition for the optimal algorithm is if the Pareto front remains unchanged after a certain number of generations. By this way, we determine the number of generation is 20 in our study. The parameters of MOGA are listed in Table 2. The number of generations and population of individuals need to be set. In addition, probability of selection gives the probability that design configurations are not changed during the evolution. In order to maintain a good diversity between points, this parameter should be kept small [26]. If the value is 1, no calculation will be performed after the initial population. It should not be increased to values higher than 0.2. In order to reduce the amount of old samples and increase new samples in next generation, probability of selection was finally set as 0.01 in our study.

Table 2. Parameters of the MOGA.

Number of Generations	20
Probability of Directional Cross-over	0.5
Probability of Selection	0.01
Probability of Mutation	0.1
DNA String mutation ratio	0.05
Random generator seed	1
Population of Individuals	50

4.2. Pareto Optimal Solutions

The multi-objective optimization procedure yields a set of optimal solution in which an improvement in one objective requires a degradation of another. In the following optimal analysis, we only discuss $\dot{m}_1 = \dot{m}_2$, and the area ratio between the upper and lower mini-channels is also equal, that is $w_1 = w_2$, $h_1 = h_2$. Figure 6 shows the optimal analysis with objective functions of $T_{s,max}$ and s_g.

Figure 6. Optimal results with objective functions of $T_{s,max}$ and s_g.

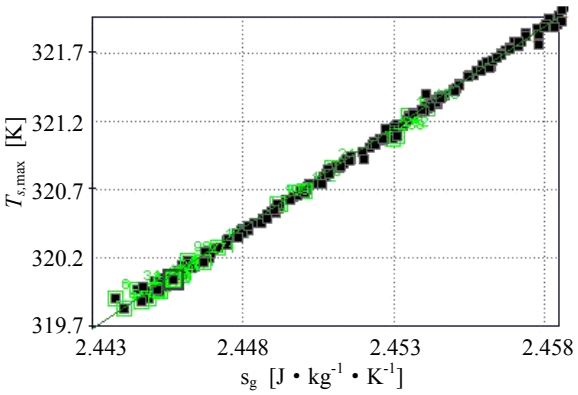

From Figure 6, we can observe that the relationship of objective functions, $T_{s,max}$ and s_g, is linear, therefore, they have a same effect on the optimal process. In the following discuss, the multiple objective optimal functions will be ΔT_s, s_g, and w_{pump}.

Three objective (ΔT_s, s_g, w_{pump}) optimal results by using MOGA, are shown in Figure 7. In Figure 7, every solid square represents a geometry design state. The solid squares marked number and green box are finally chosen optimal solutions. In order to show the Pareto front clearly, we take the 2-D projection of Figure 7, as shown in Figures 8 and 9.

Figure 7. Three objective optimal results.

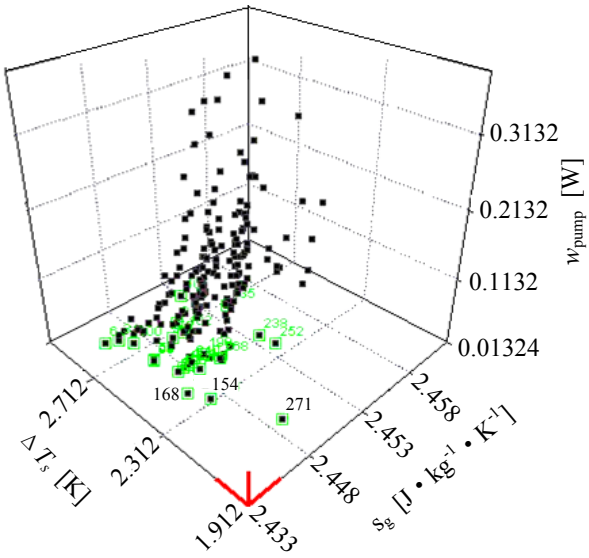

Figure 8. 2D projection of ΔT_s and s_g from three objective optimal results.

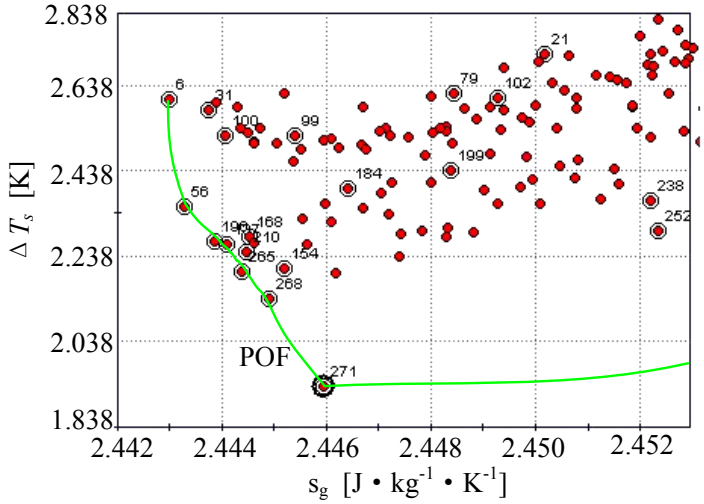

Figure 9. 2D projection of w_{pump} and s_g from three objective optimal results.

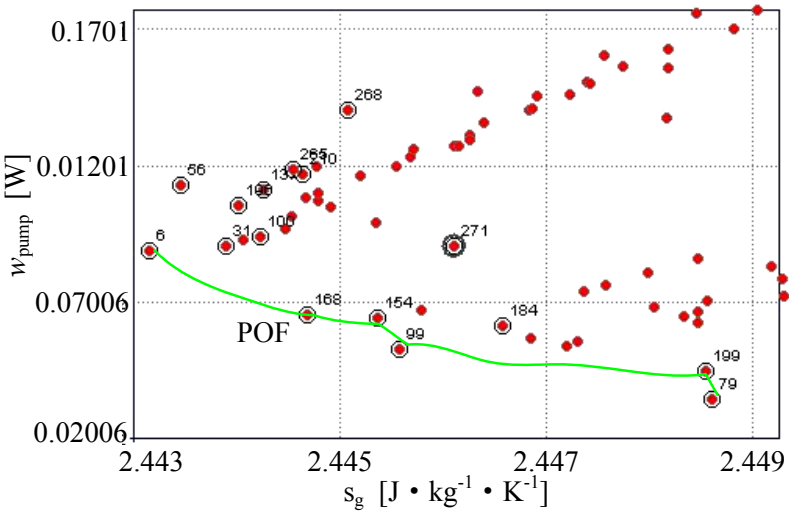

From Figures 8 and 9, we can clearly observe that:

(1) The design state points, 6, 56, 196, 137, 265, 268, 271, are on the Pareto front of ΔT_s and s_g in Figure 8, and 168, 154, 210, 137 are very close to the Pareto front.
(2) The design state points, 6, 168, 154, 99, 199 are on the Pareto front of w_{pump} and s_g in Figure 9, and 265, 271 are close to the Pareto front.

By analyzing the optimal results, we know that the optimal objective function, $T_{s,max}$ is satisfied very well in most of optimal cases, but the temperature uniformity, ΔT_s, is not. While ΔT_s is strictly limited in our optimal design due to its special application requirement, we mostly focus on the objective function of temperature uniform. We finally recommend some optimal structures for the design of the stacked mini-channel heat sink, and they are 271, 154 and 168. The details of these three points are listed in Table 3. Figures 10 and 11 show the numerical calculation results for state point 271.

Table 3. Detail information of chosen state points.

Number	h [$\times 10^{-3}$ m]	w [$\times 10^{-3}$ m]	n	ΔT_s [K]	s_g [J·kg^{-1}·K^{-1}]	w_{pump} [$\times 10^{-2}$ W]	a_2 [$\times 10^{-3}$ m]	L_y [$\times 10^{-3}$ m]
271	4.8	0.6	50	1.935	2.446	9.05	1.20	12.6
154	4.8	0.6	70	2.211	2.446	6.402	0.77	12.6
168	4.7	0.6	70	2.283	2.445	6.559	0.77	12.5

Figure 10. Cross-sectional temperature contour at $x = L_x/2$ for state point 271.

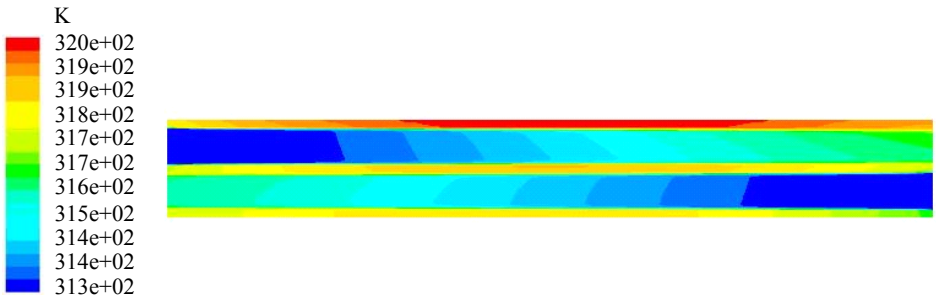

Figure 11. Cross-sectional velocity contour at $x = L_x/2$ for state point 271.

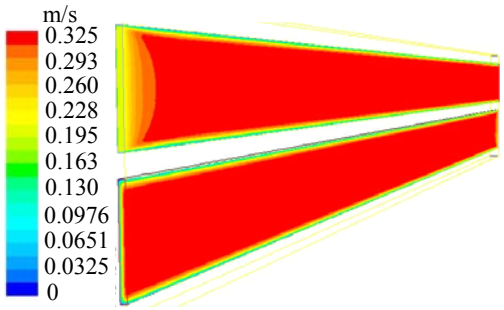

Figures 10 and 11 show the cross-sectional temperature and velocity contour at $x = L_x/2$ for state point 271. From the two figures, we can observe that:

(1) In Figure 10, ΔT_s = 1.935 K, so the temperature uniformity requirement on the heat source surface can be satisfied very well.

(2) The max temperature exists at the middle of the heat source surface due to the double-channel cooling channel arrangement.
(3) The flow temperature at the outlet is 317 K, and it is far less than 333 K.
(4) In the Figure 11, the flow velocity can quickly reach its uniform velocity after a very short distance from the inlet, so the flow can be assumed as a fully developed laminar flow at the most positions.

5. Conclusions

For the stacked mini-channel heat sink structure cooled by a small quantity of coolant, a multiple optimal design was studied in this paper in order to achieve a good temperature uniformity over its heat sink surface. In this thermal design, the objective functions were chosen as ΔT_s, s_g, $T_{s,max}$ and w_{pump}, and the optimal design variables were the mini-channel geometries. To use the entropy generation minimization method, we deduced the entropy generation in the stacked mini-channel heat sink. MOGA was used to minimize multiple objective functions subject to constraints. The Pareto-optimal solutions were obtained for global optimization by using MOGA and Fluent solver together, and then the Pareto front was located.

By analyzing the preliminary optimal results, we can know that there is a linear relationship between $T_{s,max}$ and s_g. This linear relationship indicates they have a same effect on the optimal process, so we just focus on discussing three objective optimal functions, ΔT_s, s_g, and w_{pump}. By using MOGA, we obtain the Pareto front of these three objectives. The multiple optimal results are a set, not a single value. If mostly focusing on the temperature uniformity, we can recommend some optimal structures to design the stacked mini-channel heat sink. The finally recommended structures are the state points of 271, 154 and 168.

Acknowledgments

The authors are grateful to the anonymous reviewers for their constructive review of the manuscript. The research is sponsored by the Aviation Science Foundation of China (2011ZC09004).

Conflicts of Interest

The authors declare no conflict of interest.

References

1. Haddad, O.; Abuzaid, M.; Al-Nimr, M. Entropy generation due to laminar incompressible forced convection flow through parallel-plates minichannel. *Entropy* **2004**, *6*, 413–426.
2. Liu, D.; Garimella, S.V. Analysis and optimization of the thermal performance of minichannel heat sinks. *Int. J. Numer. Methods Heat Fluid Flow* **2005**, *15*, 7–26.
3. Pritish, R.P.; Srinath, V.E.; Khai, N. Multi-layer mini-channel and ribbed mini-channel based high performance cooling configurations for automotive inverters—Part A: Design and evaluation. *J. Therm. Sci. Eng. Appl.* **2013**, *5*, 1–13.

4. Hung, T.C.; Sheu, T.S.; Yan, W.M. Optimal thermal design of microchannel heat sinks with different geometric configurations. *Int. Commun. Heat Mass Transf.* **2012**, *39*, 1572–1577.
5. Hassel, B.; Ortega, A. Analysis of multi-layer mini- and micro-channel heat sinks in single phase flow using one and two equation porous media models. *Heat Transf. Eng.* **2011**, *32*, 1–9.
6. Bowers, M.B.; Mudawar, I. High flux boiling in low flow rate, low pressure drop mini-channel and micro-channel heat sinks. *Int. J. Heat Mass Transf.* **1994**, *37*, 321–332.
7. Wei, X.J.; Joshi, Y. Stacked microchannel heat sinks for liquid cooling of microelectronic components. *J. Electron. Package* **2004**, *126*, 60–66.
8. Wei, X.J.; Joshi, Y. Optimization study of stacked mini-channel heat sinks for mini-electronic cooling. *IEEE Trans. Compon. Package Technol.* **2003**, *26*, 55–61.
9. Hung, T.C.; Yan, W.M.; Wang, X.D.; Huang, Y.X. Optimal design of geometric parameters of double-layered microchannel heat sinks. *Int. J. Heat Mass Transf.* **2012**, *55*, 3262–3272.
10. Hung, T.C.; Yan, W.M.; Li, W.P. Analysis of heat transfer characteristics of double-layered microchannel heat sink. *Int. J. Heat Mass Transf.* **2012**, *55*, 3090–3099.
11. Dixit, P.; Lin, N.; Miao, J.; Wong, W.K.; Teo, K.C. Concept and Analytical Analysis of Silicon Mini/Nanopillars Based 3-D Stacked Minichannel Heat Sink for Advanced Heat Dissipation Applications. In Proceedings of the Electronic Components and Technology Conference, Sparks, NV, USA, 29 May–1 June 2007; pp. 1149–1154.
12. Liu, Y.L.; Luo, X.B.; Liu, W. Cooling behavior in a novel heat sink based on multilayer staggered honeycomb structure. *J. Energy Power Eng.* **2010**, *4*, 22–28.
13. Toh, K.C.; Chen, X.Y.; Chai, J.C. Numerical computation of fluid flow and heat transfer in minichannels. *Int. J. Heat Mass Transf.* **2002**, *45*, 5133–5141.
14. Shao, B.D.; Wang, L.F.; Cheng, H.M.; Li, J. Optimization and numerical simulation of multi-layer minichannel heat sink. *Procedia Eng.* **2012**, *31*, 928–933.
15. Wang, X.Q.; Mujumdar, A.; Yap, C. Numerical analysis of blockage and optimization of heat transfer performance of fractal-like microchannel nets. *J. Electron. Packag.* **2006**, *128*, 38–45.
16. Jeevan, K.; Quadir, G.A.; Seetharamu, K.N.; Azid, I.A.; Zainal, Z.A. Optimization of thermal resistance of stacked micro-channel using genetic algorithms. *Int. J. Numer. Methods Heat Fluid Flow* **2005**, *15*, 27–42.
17. Shao, B.D.; Wang, L.F.; Li, J.Y.; Cheng, H.M. Multi-objective optimization design of a mini-channel heat sink using adaptive genetic algorithm. *Int. J. Numer. Methods Heat Fluid Flow* **2011**, *21*, 353–364.
18. Foli, K.; Okabe, T.; Olhofer, M.; Jin, Y.; Sendhoff, B. Optimization of mini heat exchanger: CFD, analytical approach and multi-objective evolutionary algorithms. *Int. J. Heat Mass Transf.* **2006**, *49*, 1090–1099.
19. Karathanassis, I.K.; Papanicolaou, E.; Belessiotis, V.; Bergeles, G.C. Multi-objective design optimization of a mini heat sink for Concentrating Photovoltaic/Thermal (CPVT) systems using a genetic algorithm. *Appl. Therm. Eng.* **2013**, *59*, 733–744.
20. Husain, A.; Kim, K.Y. Enhanced multi-objective optimization of a minichannel heat sink through evolutionary algorithm coupled with multiple surrogate models. *Appl. Therm. Eng.* **2010**, *30*, 1683–1691.

21. Hassan, M.; Sadri, R.; Ahmadi, G.; Dahari, M.B.; Kazi, S.N.; Safaei, M.R.; Sadeghinezhad, E. Numerical study of entropy generation in a flowing nanofluid used in micro- and mini-channels. *Entropy* **2013**, *15*, 144–155.
22. Ansari, D.; Husain, A.; Kim, K.Y. Multiobjective optimization of a grooved mini-channel heat sink. *IEEE Trans. Compon. Package Technol.* **2010**, *15*, 767–776.
23. Khan, W.A.; Culham, J.R. Optimization of minichnnel heat sinks using entropy generation minimization method. *IEEE Trans. Compon. Package Technol.* **2009**, *32*, 243–251.
24. Deb, K. *Multi-Objective Optimization Using Evolutionary Algorithms*; Wiley: London, UK, 2001.
25. Jaluria, Y.; Simulation-based optimization of thermal systems. *Appl. Therm. Eng.* **2009**, *29*, 1346–1355.
26. Poles, S.; Geremia, P.; Campos, F.; Weston, S.; Islam, M. MOGA-II for an Automotive Cooling Duct Optimization on Distributed Resources. In Proceedings of the 4th International Conference on Evolutionary Multi-Criterion Optimization (EMO'07), Matsushima, Japan, 5–8 March 2007; Springer: Berlin/Heidelberg, Germany, 2007; pp. 633–644.
27. FLUENT, v. 6.3; Software for fluid simulation; Fluent, Inc.: New York, NY, USA, 2006.
28. Shah, R.K.; London, A.L. *Laminar Flow Forced Convection in Ducts*; Academic Press: New York, NY, USA, 1978.